NANO LETTERS

2008
Vol. 8, No. 8
2271-2276

Glass Transition of Polymer−Nanocrystal Thin Film Mixtures: Role of Entropically Directed Forces on Nanocrystal Distribution

Abraham Arceo, Luciana Meli, and Peter F. Green*

Department of Materials Science and Engineering, University of Michigan, Ann Arbor, Michigan 48109

Received April 2, 2008

ABSTRACT

The connection between the average properties of a polymer/nanocrystal hybrid material and the nanocrystal spatial distribution is shown. Specifically, a property such as the glass transition temperature, T_g, is shown to vary by a much as 65 °C through only changes in the spatial distribution of the nanocrystals. Considerable control can be exercised over the nanoparticle spatial distribution. In addition, we show that while the T_g of a thin film hybrid material may be enhanced in relation to the pure bulk system, the bulk nanocomposite analog shows a reduction in T_g. These findings have broad implications with regard to the design of materials with required properties.

Polymer/nanoparticle mixtures, hybrid materials, often exhibit unusual property enhancements compared with their pure polymer analogs, even at low nanoparticle concentrations.[1,2] The property enhancements exhibited by these materials are in part attributed to the large surface area to volume ratio of the nanoparticles, and to relative nanoparticle−polymer, polymer−polymer, and nanoparticle−nanoparticle interactions. These collective interactions are responsible for improvements not only in the mechanical behavior (e.g.: strength, toughness) but also changes in the glass transition, dynamics, and other properties.[3]

However, particle−particle aggregation is responsible for a heterogeneous particle distribution throughout these materials; this heterogeneous distribution makes it difficult to control the properties of the system. Strong, favorable, interactions between chain segments and particles are responsible for enhancements in the local monomer density in the vicinity of the particles relative to the bulk.[4−8] This increase in monomer density is associated with a decrease of the configurational freedom and of the dynamics of the chains surrounding the filler.[5−7,9] Hence, local heterogeneities in properties such as the glass transition and the local dynamics are connected to the heterogeneities in the structure. The implication is average properties, such as the average glass transition temperature, the average dynamics, and the mechanical properties of the system,[10,11] are strongly influenced by the structural heterogeneities of the system.

Since the properties of the material are sensitive to the spatial distribution of nanoparticles throughout the system, the primary challenge is associated with attaining control of the size and dispersion of the nanoparticles throughout the system. In this paper, we study thin, $h \approx 100$ nm thick, film polystyrene (PS) and PS-grafted gold nanoparticle mixtures; the nanoparticle distribution within the sample is associated with the degrees of polymerization P and N, of the host chains and grafted chains, respectively, and σ, the grafting density. We show how the nanoparticle size and spatial distribution strongly influences the glass transition of the film; T_g can be shifted as much as 65 °C with changes of only the nanoparticle distribution. Moreover, we show that while the T_g of a thin film PS/nanoparticle may be enhanced in relation to pure PS, the bulk PS/nanoparticle analog exhibits a reduction in T_g.

The grafted nanoparticles were prepared as follows. Gold nanocrystals were synthesized using a modified version of the procedure first reported by Brust et al.[12] Three separate reaction batches were prepared; the first one was terminated at an early stage during the reaction to obtain nanoparticles with an average diameter of $R_{core} = 1.8$ nm, as measured using scanning transmission electron microscopy (STEM), described below. The surface of these nanoparticles was grafted with thiol-terminated polystyrene chains (Polymer Source, Inc.) with degree of polymerization $N = 10$. The second batch was allowed to react until the nanoparticle core size reached an average value of $R_{core} = 5$ nm. This batch was grafted with polystyrene ligands of $N = 480$. The third

* Corresponding author.

10.1021/nl800932u CCC: $40.75
Published on Web 07/23/2008

Table 1. Characteristics of the Film Nanocomposites

sample	nanoparticle	P	N	R_{Au}/R_g	R_e/R_g	$\sigma N^{1/2}$	$(N/P)^2$
A	Au(5)-PS_{10}-SH	1462	9.6	0.24	0.48	1.13	$4.32*10^{-5}$
B	Au(5)-PS_{481}−SH	1462	481	0.23	2.6	9.55	0.11
C	Au(2)-PS_{10}-SH	1462	9.6	0.088	0.22	1.67	$4.32*10^{-5}$

series of nanoparticles of $R_{core} = 5$ nm were grafted with PS chains of $N = 10$. The nanoparticle solutions were subsequently cleaned by precipitating them from the solution using ethanol. This procedure was repeated at least 8 times. After cleaning, thermogravimetric analysis was performed to obtain the grafting densities of the nanoparticles.

The average size of the particles was obtained using a JEOL 2010 transmission electron microscope (TEM) operating at an accelerating voltage of 200 KV in scanning mode using a high-angle annular dark-field detector (HAADF). TEM grids were prepared by evaporating dilute solutions of the nanoparticles. After imaging, the diameter of the particles was estimated from the measurement of over 300 particles, using Image J software.

After characterization, the nanoparticle solutions were mixed with previously prepared toluene solutions of polystyrene homopolymer (Pressure Chemical, Inc.) of Mn = 130 000 g/mol, and 152 000 g/mol. It is worth noting that for the purposes of this experiment the difference in molecular weights of these matrices is negligible (i.e., their unperturbed radius of gyration is approximately the same). The nanocomposite solutions had compositions ranging from 0.1 to 5% by weight of gold cores for the case of the nanoparticles with 1000 g/mol PS ligands ($N = 10$), and from 0.1 to 10% for the nanoparticles with 50 000 g/mol ($N = 480$) ligands. Each of the nanocomposites can be characterized by the relative size of the ligand (N, which denotes number of monomer units) and matrix chains (denoted as P), as well as by the ratio of R_e/R_g (see Table 1). Here, R_g refers to the unperturbed radius of gyration of the host chains, and R_e refers to the effective particle radius, which is given by the gold core radius plus the brush thickness. The brush thickness of the nanoparticles was obtained by measuring interparticle separation distance on TEM samples of the pure particles.

The nanocomposite solutions described above were spin-coated on Si_3N_4 substrates (WaferNet, Inc.) to obtain film thicknesses between 100 and 115 nm. The thickness of the films was measured by ellipsometry using a J. A. Woollam M-44 variable-angle spectroscopic ellipsometer with a visible light source (wavelengths from 400 to 720 nm). After spin coating, the resulting films were placed in an oven at 80 °C for 48 h under a vacuum to remove residual solvent. At this point, it is important to note that the samples were not annealed at a higher temperature to avoid nanoparticle coarsening which has been observed for similar systems.

The depth profile of gold within the samples was characterized using dynamic secondary ion-mass spectroscopy (DSIMS), measured at the University of California at Santa Barbara with a Physical Electronics 6650 Quadropole instrument. For DSIMS analysis, a second deuterated PS film was floated on top of the nanocomposite films to serve as a marker for the location of the free surface. Sputtering was then accomplished with a cesium primary ion beam monitoring negative ions of Au, Si, dH, and C. The sputtering time was converted to a depth scale using the depth profile and the total film thickness, measured from ellipsometry. The gold concentration is normalized by the total number of gold counts. Finally, the degree of dispersion in the x-y plane of the films was characterized by obtaining STEM images of similar films cast on transparent silicon nitride membrane windows (SPI supplies).

After annealing, the samples were placed in a custom-made heating stage, and their thickness was measured at regular intervals of 10 °C during the experiment. Three measurements were taken at each temperature. The heating rate was 1 °C/min, and the temperature ramp started at 30 °C and ended at 170 °C. Film thickness was determined by fitting the ellipsometric angles, Δ and Ψ, to a composite layer (effective medium approximation) of a Cauchy model and gold, using the Maxwell−Garnett model. T_g was determined by fitting straight lines through the data in the glassy and rubbery regions, respectively; the temperature at which these lines intersect denotes the glass transition.

The data in Figure 1 provide the key findings in this paper: for a given nanoparticle weight fraction, the T_g can change tens of degrees. The glass transition exhibits a strong dependence not only on composition but also on particle size and grafting chain length, as shown in Figure 1. For convenience we will label the three series of samples as A, B, and C, as described in Table 1. The T_g of the C samples

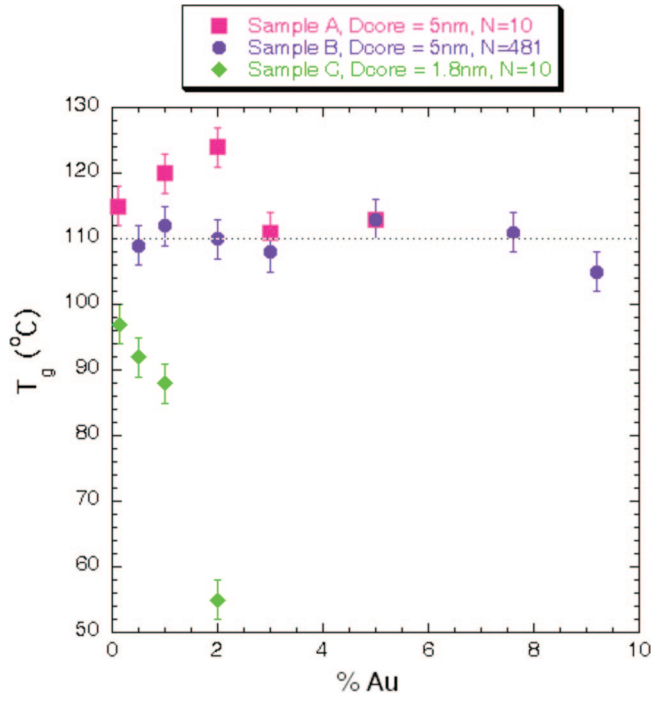

Figure 1. Dependence of T_g as a function of nanoparticle content. All films have thicknesses between 100 and 115 nm.

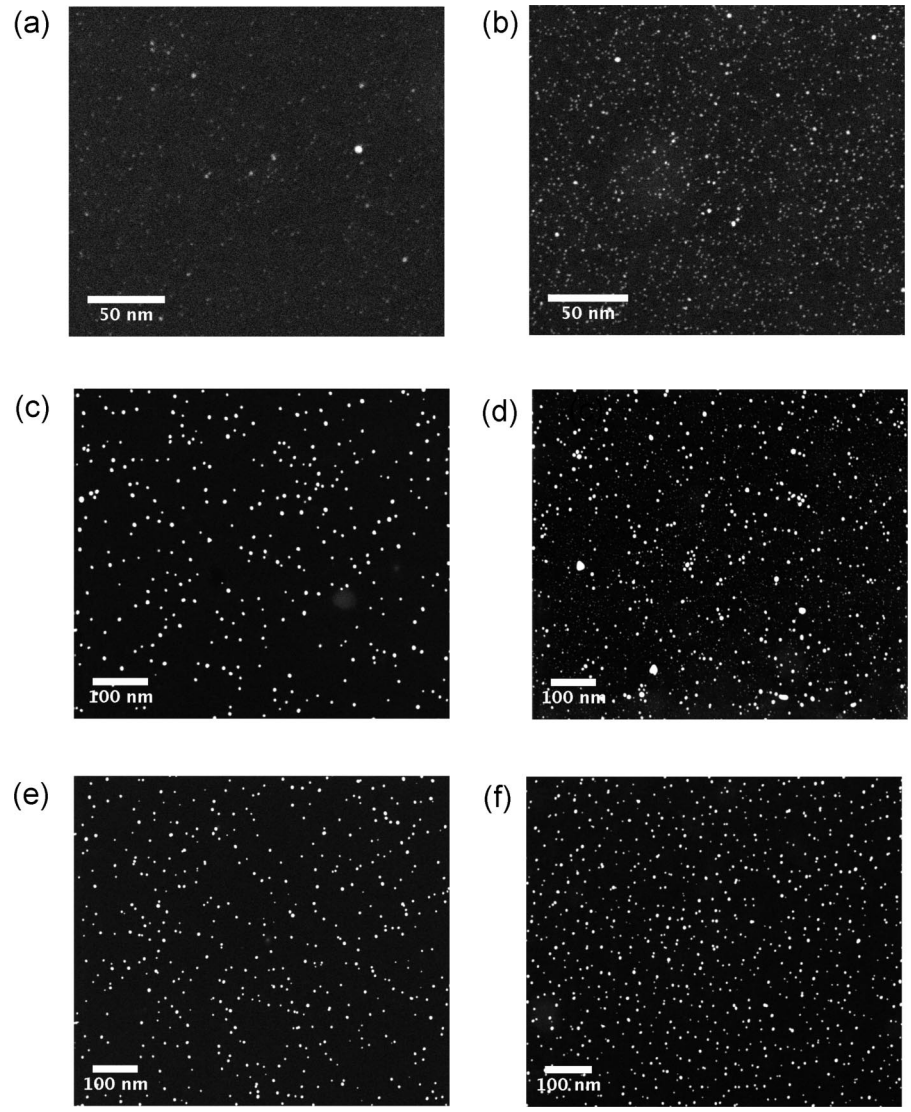

Figure 2. STEM images taken for PS/PS-Au nanocomposites. The first row (a,b) corresponds to nanocomposites with gold nanoparticles characterized by $D_{core} = 1.8$ nm and $N = 10$ (Sample C). The second row (c,d) corresponds to nanocomposites with gold nanoparticles characterized by $D_{core} = 5$ nm and $N = 10$ (Sample A). The third row (e,f) shows the nanocomposites formed with nanoparticles characterized by $D_{core} = 5$ nm and $N = 480$ (Sample B). The first column shows gold concentrations of 1% w/w, whereas the second column shows images for gold concentrations of 5% w/w.

(small core, short ligands) decreases rapidly with increasing nanoparticle mass fraction. At 2%, the T_g dropped 55 °C. For the B samples (large core, long ligands), the glass transition remained somewhat insensitive to nanoparticle content. The glass transition of the A samples (large core, short ligands) initially increased, reaching a maximum at a concentration of ~2% and then decreased at higher nanoparticle content.

A first step toward understanding our results is to examine the distribution of the nanoparticles in the films using STEM, which provides information about the lateral distribution, and by DSIMS, which provides information about the distribution of gold particles, normal to the interfaces. Figure 2 shows the in-plane images of the nanocomposites. It can be seen that, in general, the nanoparticles are well-dispersed laterally, except in the case of the 5% w/w A samples, where a few clusters are observed. To get further insight, it is instructive to consider the DSIMS measurements of the gold depth profile of these samples containing 5% w/w of nanoparticle cores (Figure 3). This depth profile of the A samples (effective size $R_e/R_g \sim 0.5$) reveals that the nanoparticles are segregated almost exclusively to the interfaces. Upon decreasing the effective size of the nanoparticles to $R_e/R_g \sim 0.22$ (C samples), we find that the nanoparticles no longer exclusively reside at the interfaces; a fraction of the particles now reside in the interior, ~22% of the total Au. Finally, the depth profile of the B samples exemplifies the effect of changing the length of the brush; in this case, the molecular weight of the ligand is more than an order of magnitude larger than that of the A samples. The DSIMS data show that this type of nanoparticle is distributed almost uniformly across the sample. The ensuing discussion will make it clear that it is more convenient to regard the difference between A and B samples as a change in brush quality, rather than a change in the effective size, R_e/R_g.

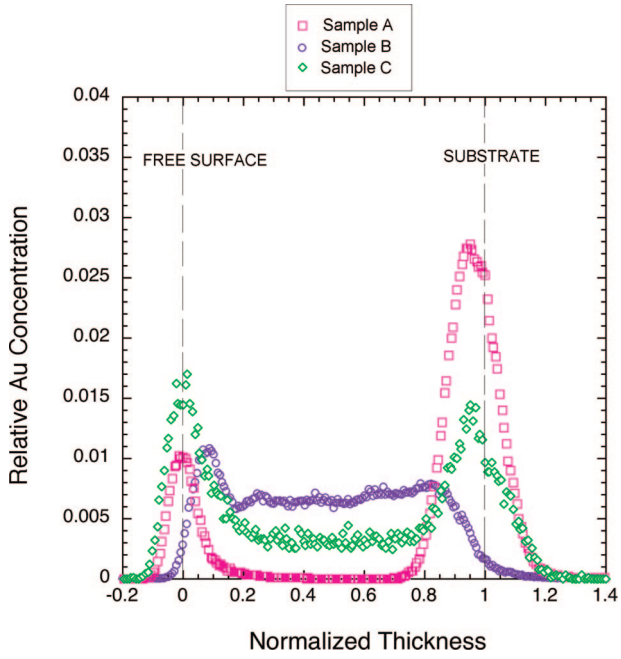

Figure 3. Depth distribution of gold in the nanocomposite films determined by DSIMS. All samples were prepared with a gold content of 5% w/w.

Now that the spatial distribution of the particles is understood, we now proceed to explain the observations in Figure 1; in doing so, we establish a direct a clear-cut connection between particle dispersion and a property of the system. The nanocrystal depth profile in the samples is primarily determined by the balance between the entropic interactions between matrix chains and the polymer coated nanoparticles, the translational entropy of the chains, and the elastic energy of the chains in the vicinity of the nanoparticles.[13–17] The entropy of mixing promotes mixing of the nanoparticles, and its contribution to the total free energy of the system increases with decreasing particle size: $F_{mix} \sim (\phi/R_{np}^3) \ln \phi$ (R_{np} is the particle diameter and ϕ is the particle volume fraction). At the same time, the host chains have to stretch in order to accommodate the particles and the stretching energy increases with increasing particle size, and this contribution to the free energy is $F_{stretch} \sim (R_{np}/R_g)^2$. Entropic constraints due to the brush/host chain interactions are significant and can favor mixing of the nanoparticles with the host chains or contribute toward phase separation between particles and host chains.

The host/brush interactions are determined by the parameters N, P and σ.[13,18] When the grafted chains are sufficiently long and the grafting density is sufficiently low, that is, $\sigma N^{1/2} < (N/P)^{1/2}$, then the host chains can interpenetrate or wet the brush layer thereby forming a so-called "wet brush." This would promote miscibility between the particles and the host chains. On the other hand, when the grafting density is very high, specifically, when $\sigma N^{1/2} > (N/P)^{1/2}$, the host chains are partially excluded from the grafted layer. This creates a driving force for the nanoparticles to aggregate in order to minimize the area of contact. We will use this information as a guide to understand the entropic interactions in our system; however, it is important to note that this relationship was derived for flat surfaces. Nevertheless, this should not be problematic as the basic physics is similar. The only difference is that a brush on a curved surface should be more penetrable by melt chains than a brush of the same grafting density on a flat surface; the grafted chains are less stretched (and therefore less tightly packed) away from the particle surface, as discussed by Meli et al.[18]

To this end, we now discuss the effect of brush quality on the depth profile of the particles in the films seen in Figure 3. A uniform degree of dispersion of the nanoparticles was obtained in the B samples. This uniformity is readily attributed to the large size of the grafted chains ($P/N = 3$), which should accommodate greater interpenetration of the matrix chains into brush layer. Interpenetration reduces the conformational entropy penalty the matrix chains would otherwise experience in the immediate vicinity of an impenetrable surface, thus promoting dispersion. Further, the curvature of the brush layer promotes a greater degree of interpenetration, as mentioned earlier.

We now turn our attention to the role of the effective nanoparticle size. Figure 3 shows that the nanoparticles in the A samples ($R_e/R_g \sim 0.5$) are primarily segregated to the interfaces. This is due to the fact that the polymer melt does not wet the short grafted chains covering the nanoparticle core; namely, $\sigma N^{1/2} \gg (N/P)^{1/2}$. Moreover, the stretching energy penalty of the chains near the nanoparticles is high for these samples, since the average dimensions of the matrix chains are comparable to the size of the nanoparticle. In contrast, while for the C samples the condition $\sigma N^{1/2} \gg (N/P)^{1/2}$ still applies (as indicated by the peaks near the interfaces in the DSIMS data), for the smaller effective size of the particles ($R_e/R_g = 0.22$), by virtue of their greater entropy of mixing (which scales as R_e^{-3}), the nanoparticles are distributed throughout the film. Further, it is important to note that the nanoparticles in the C samples do not form aggregates, at least within the range of nanoparticle concentrations studied.

The observations regarding glass transition behavior, Figure 1, may now be understood in terms of the nanoparticle distribution within the samples. In the C samples, the particles are small compared with R_g ($R_e/R_g \ll 1$) and reside in the interior of the film. Since the host chains and the particles are nonwetting, there is a local depletion of chain segments in the vicinity of the particles, compared with the bulk which would increase in an oscillatory manner until it reaches the bulk value (for cases where the chain segments strongly adsorb to the particles, the local monomer density is highest at the point of contact). An alternate way of thinking about this effect is in terms of an increase in the free volume compared with that of a neat homopolymer sample, that is, simple "packing" argument. The increased free volume would be associated with a decrease in the glass transition of the samples. On the other hand, the T_g of the B samples exhibited no dependence on nanoparticle concentration as the grafted chains are long and are sufficiently interpenetrated by the host chains. Hence the "packing" of the nanoparticles in this system is more efficient than in the other two and is

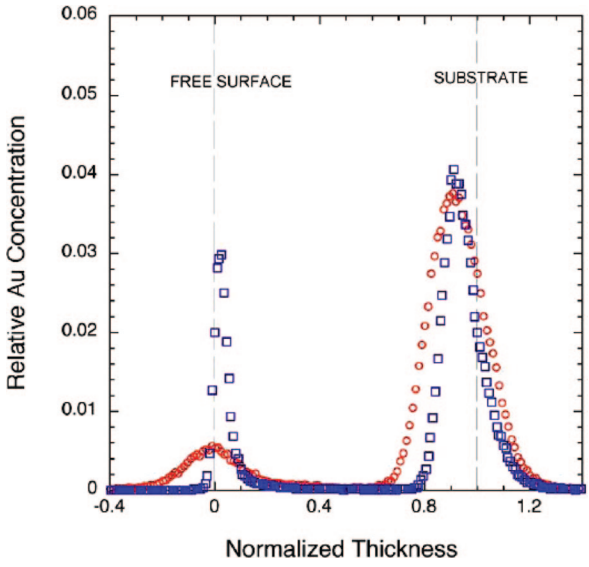

Figure 4. Comparison of the Au depth profile of two different concentrations of samples prepared with nanoparticles with core diameter of 5 nm, and ligand degree of polymerization, $N = 10$, squares represent data for 1% w/w, and circles represent data for 5% w/w.

not expected to perturb the local monomer density near the surface of the particles.

The presence of a maximum in the measured T_g in the A samples, denotes a competition between opposing forces present in the system. The initial increase in T_g can be attributed to the fact that the nanoparticles segregated to the interfaces. At low concentrations, the interior of the film remains devoid of particles. We suspect that the nanoparticles act as flat layers at the interfaces, restricting the configurational freedom of host chains, compared with the influence of a free surface. However, with increasing nanoparticle concentration, the DSIMS data (Figure 4) show increasing amounts of nanoparticles begin to penetrate further into the film (the "nanoparticle-free" region of an A sample with 5 wt % Au is considerably smaller than that with just 1%); this would necessarily lead to a decrease in T_g.

We also examined the glass transition of bulk polymer/nanoparticle mixtures, where interfaces are not important, to get further insight into the foregoing observations. The nanoparticles with short ligands, samples A and C, were used, so the host chains and the nanoparticles are nonwetting. The bulk samples exhibited decreases in the glass transition, which is consistent with an increase on the free volume of the system associated with nonwetting nanoparticles. These observations are noteworthy as the films can exhibit a larger glass transition temperature than the bulk in these systems, due to segregation at the interfaces. Parenthetically, numerous studies of the T_g of thin PS films show that the T_g decreases with decreasing film thickness; however, that thickness range is less that 40 nm, which is thinner than the samples examined in this study.[19,20] This present study shows the role of the interface is important as the segregation of nanoparticles to the interface affects the glass transition.

We have clearly shown how the nanoparticle size and spatial distribution within a thin film polymer/nanoparticle system can have a significant influence on a property, such as the glass transition, shifting it as much as 65 °C, at constant weight fraction of nanoparticles. The location of the nanoparticles is dictated by the host chain degree of polymerization, P, the grafted chain density of the nanoparticle, σ, the degree of polymerization of the grafted chains, N, and the nanoparticle/host chain size ratio (R_e/R_g). When the nanoparticles are small and the grafting density is high, the P chains are entropically restricted from interpenetrating the brush layer; however, the translational entropy is largely responsible for mixing of the nanoparticles throughout the interior of the film. Under these conditions, the T_g decreases substantially with nanoparticle weight fraction ϕ, largely because of the increase in free volume (monomer depletion in the vicinity of the particles in relation to the bulk) of the system. When the chain size ratio (R_e/R_g) is increased from 0.322 to 0.48, the particles exclusively reside at the interfaces. This is because the elastic contribution to the free energy is large and the particles cannot be accommodated within the polymer host. Hence, the nanoparticles now segregate to the interfaces largely to minimize the interfacial free energy. Under these conditions, the T_g increases. However, the bulk analogues of these samples exhibit a lower T_g, as the particles remain in the interior of the sample, effectively lowering the free volume. However, when N increases, the P chains are able to interpenetrate the brush layer, and the particles have no influence on the T_g of the bulk.

The rationale behind these findings suggests a strategy to accurately design the microstructure of polymer/nanoparticle systems and is the subject of a separate paper.[18] Further experiments are under way in order to fully sample the vast parameter space that characterizes this system.

Acknowledgment. This work was supported by the US Department of Energy, Office of Science, BES Program DOE#DE-FG02-07ER 46412.

References

(1) Chan, C.-M.; Wu, J.; Li, J.-X.; Cheung, Y.-K. *Polymer* **2002**, *43*, 2981.
(2) Sariciftci, N. S.; Simolowitz, L.; Heeger, A. J.; Widl, F. *Science* **1992**, *258*, 1474.
(3) Krishnamoorti, R.; Vaia, R. A.; Giannelis, E. P. *Chem. Mater.* **1996**, *8*, 1728.
(4) Desai, T.; Keblinski, P.; Kumar, S. K. *J. Chem. Phys.* **2005**, *122*, n/a.
(5) Smith, G. D.; Bedrov, D.; Li, L. W.; Byutner, O. *J. Chem. Phys.* **2002**, *117*, 9478.
(6) Starr, F. W.; Schroder, T. B.; Glotzer, S. C. *Phys. Rev. E* **2001**, *6402*, n/a.
(7) Starr, F. W.; Douglas, J. F.; Glotzer, S. C. *J. Chem. Phys.* **2003**, *119*, 1777.
(8) Vacatello, M. *Macromolecules* **2001**, *34*, 1946.
(9) Pryamitsyn, V.; Ganesan, V. *Macromolecules* **2006**, *39*, 844.
(10) Kropka, J. M.; Garcia-Sakai, V.; Green, P. F. *Nano Lett.*, in press.
(11) Kropka, J. M.; Putz, K. W.; Pryamitsyn, V.; Ganesan, V.; Green, P. F. *Macromolecules* **2007**, *40*, 5424.
(12) Brust, M.; Walker, M.; Bethell, D.; Schiffrin, D. J.; Whyman, R. *J. Chem. Soc., Chem. Commun.* **1994**, 801.

(13) Ferreira, P. G.; Ajdari, A.; Leibler, L. *Macromolecules* **1998**, *31*, 3994.
(14) Wijmans, C. M.; Zhulina, E. B.; Fleer, G. J. *Macromolecules* **1994**, *27*, 3238.
(15) Gast, A. P.; Leibler, L. *Macromolecules* **1986**, *19*, 686.
(16) Hasegawa, R.; Aoki, Y.; Doi, M. *Macromolecules* **1996**, *29*, 6656.
(17) Zheng, L.; Xie, A. F.; Lean, J. T. *Macromolecules* **2004**, *37*, 9954.
(18) Meli, L.; Arceo, A.; Green, P. F., submitted.
(19) Forrest, J. A.; Dalnoki-Veress, K.; Dutcher, J. R. *Phys. Rev. E* **1997**, *56*, 5705.
(20) Forrest, J. A.; Dalnoki-Veress, K.; Stevens, J. R.; Dutcher, J. R. *Phys. Rev. Lett.* **1996**, *77*, 2002.

NL800932U